DOI 10.1007/s10812-023-01481-2
Journal of Applied Spectroscopy, Vol. 89, No. 6, January, 2023 (Russian Original Vol. 89, No. 6, November–December, 2022)

STRUCTURAL AND SPECTROSCOPIC CHARACTERIZATION OF 3-[4-(TRIFLUOROMETHYL)PHENYL]-3a,4,8,8a-TETRAHYDRO-6H-[1,3] DIOXEPINO[5,6-d][1,2]OXAZOLE COMPOUND: AN EXPERIMENTAL AND DENSITY FUNCTIONAL THEORY STUDY

H. Gümüş,[a] N. Tekin,[b] and Y. S. Kara[b,*]

UDC 539.143.43;543.42/.44

To better understand the molecular definition of 3-[4-(trifluoromethyl)phenyl]-3a,4,8,8a-tetrahydro-6H-[1,3] dioxepino[5,6-d][1,2]oxazole (OXE–OXA) compound, we examined its molecular geometric structure and spectroscopic properties in detail. First, we determined the OXE–OXA compound's crystal structure using single-crystal X-ray diffraction data, then we grew a single crystal of the OXE–OXA compound using the slow evaporation solution magnification technique at room temperature with ethanol. It was found that the OXE–OXA compound crystallizes in the monoclinic crystal system with the noncentrosymmetric space group P1 21/n1. We performed the theoretical calculations for OXE–OXA compound at the B3LYP/6-311++G(d,p) and HSEh1PBE/6-311++G(d,p) levels of the density functional theory method. According to the comparison of our obtained data, the experimental ^{1}H and ^{13}C nuclear magnetic resonance chemical shifts were in strong agreement with the values for simulated chemical shifts. Later, we investigated the experimental FT-IR and theoretical IR spectrum of OXE–OXA compounds in the 4000–400 cm^{-1} region.

Keywords: *crystal structure, X-ray diffraction, oxazole, infrared spectrum, nuclear magnetic resonance, density functional theory.*

Introduction. Dioxepino and isoxazole rings, which are important parts of heterocyclic compounds, both exist in the molecular structure examined in this study. Dioxepino derivatives have a wide variety of pharmacological activities such as antihyperglycemic [1] antiviral, antimalarial, anticancer, and anti-infective [2], antimalarial [3] antimicrobial [4] antifungal [5] antibacterial [6] anti-HIV [7], antitoxoplasma gondii [8], and cytotoxic [9]. Our literature search revealed that isoxazole rings and their derivatives are reported to have antibacterial [10], antimicrobial, antioxidant, anticancer [11], antianthelmintic [12], analgesic, anti-inflammatory [13], anticonvulsant and antiplatelet activities [14].

In our previous study, we synthesized and characterized 11 novel 3-(substituted phenyl)-3a,4,8,8a-tetrahydro-1,3-dioxepino[5,6-d][1,2] isoxazoles with by FT-IR, ^{1}H NMR, ^{13}C NMR, and HRMS [15]. In the study, we did not investigate the theoretical or spectroscopic analyses of any derivatives of 3-(substituted phenyl)-3a,4,8,8a-tetrahydro-1,3-dioxepino[5,6-d] [1,2] isoxazoles in detail. To eliminate this deficiency, we investigated the structural and spectroscopic analysis of an 3-[4-(trifluoromethyl)phenyl]-3a,4,8,8a-tetrahydro-6H-[1,3]dioxepino[5,6-d][1,2]oxazole (OXE–OXA) compound using the density functional theory (DFT) method:

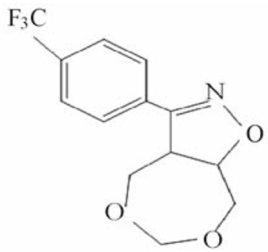

OXE–OXA

*To whom correspondence should be addressed.

[a]Golcuk Vocational School at Kocaeli University, Kocaeli, Turkey; [b]Department of Chemistry, Science and Art Faculty, Kocaeli University, Umuttepe, Kocaeli, Turkey; email: yesimkara@kocaeli.edu.tr. Abstract of article is published in Zhurnal Prikladnoi Spektroskopii, Vol. 89, No. 6, p. 897, November–December, 2022.

Experimental and Calculations. An OXE–OXA compound was synthesized according to the literature [15]. We purified and separated the synthesized product using silica gel (230–400 mesh, 0.040–0.063 mm, Merck) through column chromatography and recorded the FT-IR spectrum of OXE–OXA compound in the solid-state in the 4000–400 cm^{-1} region using a Bruker Alpha II spectrometer. ^{1}H NMR and ^{13}C NMR spectra and the substituent chemical shifts were recorded by a Bruker Avance III (400 MHz) High Performance Digital FT-NMR spectrometer with tetramethylsilane (TMS) as an internal standard in deuterochloroform ($CDCl_3$).

A single crystal of the OXE–OXA compound was grown using the slow evaporation solution growth technique at room temperature. We prepared a saturated solution of the OXE–OXA compound in ethanol and stirred the solution for 3–5 h at room temperature to obtain a homogeneous solution. A flask containing the resulting solution was tightly covered with a thin layer of polyethylene to control the rate of evaporation of the solvent and kept intact in a dust-free environment. We collected the single crystal of the macroscopically flawless OXE–OXA compound approximately 20 days later.

The single-crystal X-ray intensity data for the OXE–OXA compound, $[C_{13}H_{12}F_3NO_3]$, were selected and diffraction data were collected with MoK_α radiation ($\lambda = 0.71073$ Å) at 296(2) K using a Bruker APEX II QUAZAR three-circle diffractometer. Indexing was performed using the package of software APEX2 [16]. Data integration and reduction were carried out with SAINT [17]. Absorption correction was performed by the multiscan method implemented in SADABS [18]. The structure was solved using SHELXT [19] and then refined by full-matrix least-squares refinements on F^2 using the SHELXL [20] in the OLEX 2 program package [21]. The aromatic and aliphatic C-bound H atoms were positioned geometrically and refined using a riding mode. Crystal structure validations and geometrical calculations were performed using Platon software [22], and Mercury software [23] was used for visualization of the cif files. Additional crystallographic data with CCDC reference No. 2100835 for the studied molecule has been deposited within the Cambridge Crystallographic Data Center.

The theoretical quantum chemical calculations for the OXE–OXA compound were computed using Gaussian 09 software [24]. The optimized geometric structure of the OXE–OXA compound was drawn by Gaussian View 5 program [25]. Theoretical calculations were performed at B3LYP/6-311++G(*d*,*p*) [26, 27] and HSEh1PBE/6-311++G(*d*,*p*) [28–31] levels of the DFT method.

Results and Discussion. *Molecular geometric structure.* The OXE–OXA compound was crystallized in the monoclinic system and *P*1 21/*n*1 space group with unit cell parameters $a = 10.314(2)$ Å, $b = 6.2515(11)$ Å, $c = 19.962(4)$ Å, $\alpha = \gamma = 90^o$ and $\beta = 100.761(16)^o$. The unit cell volume (V) is 1264.5(4) $Å^3$. The experimental molecular geometric structure and atomic numbering of the OXE–OXA compound and its optimized geometric structure are shown in Fig. 1. The crystallographic data are listed in Table 1. This crystal structure with more than one molecule in the unit cell has helped in understanding the interactions among atoms in order to guide the design of technologically useful materials.

We conducted our computational investigations of the OXE–OXA compound using the DFT/B3LYP/6-311++G(*d*,*p*) and DFT/HSEh1PBE/6-311++G(*d*,*p*) methods in the gas phase under vacuum. The solid-state molecular structure determined by single-crystal X-ray diffraction and the calculated geometric parameters (bond lengths, bond angles, and dihedral angles) are compared in Table 2.

The correlation graphics of the calculated and experimental bond lengths and bond angles for the OXE–OXA compound are shown in Fig. 2. The correlation among the OXE–OXA compound's theoretical (B3LYP/6-311++G(*d*,*p*)) and experimental bond lengths and bond angles are 0.8999 and 0.9277, respectively.

From geometric parameters, theoretical bond lengths (for C–C) were found in the 1.386–1.550 Å and 1.388–1.541 Å ranges at B3LYP and HSEh1PBE, respectively. Experimental bond lengths (for C–C) were seen in the 1.380(5)–1.536(5) Å range. The experimental C_4–C_5, C_{11}–F_3, C_6–N_1, and N_1–O_1 bond lengths were 1.512(5), 1.324(6), 1.275(4), and 1.397(4) Å, respectively. Our calculated bond lengths were 1.539, 1.359, 1.281, and 1.381 Å, respectively, for the B3LYP and 1.530, 1.389, 1.279, and 1.363 Å, respectively, for the HSEh1PBE. The experimental N_1–O_1–C_1 bond angle was 109.8(2) ^{o} and this angle was seen at 110.474^o for the B3LYP and 110.601^o for the HSEh1PBE. We noted that the experimental results belong to the solid phase and the theoretical calculations, in this study can be classified as favorable, because they are supported by the experimental data, which can be seen in Table 1. The largest differences between the experimental and theoretical bond length and bond angle values are about 0.018 Å and 2.97^o, respectively. As can be seen, there was a strong agreement between the experimental and calculated geometric parameters.

Vibrational (IR) spectra. To better understand OXE–OXA compound's spectroscopic structure, we conducted detailed experimental and theoretical analyses. OXE–OXA compound's IR spectrum was performed using two different DFT methods. We performed vibrational frequency calculations for OXE–OXA compound using the B3LYP and HSEH1PBE methods with the 6-311++G(*d*,*p*) basis set.

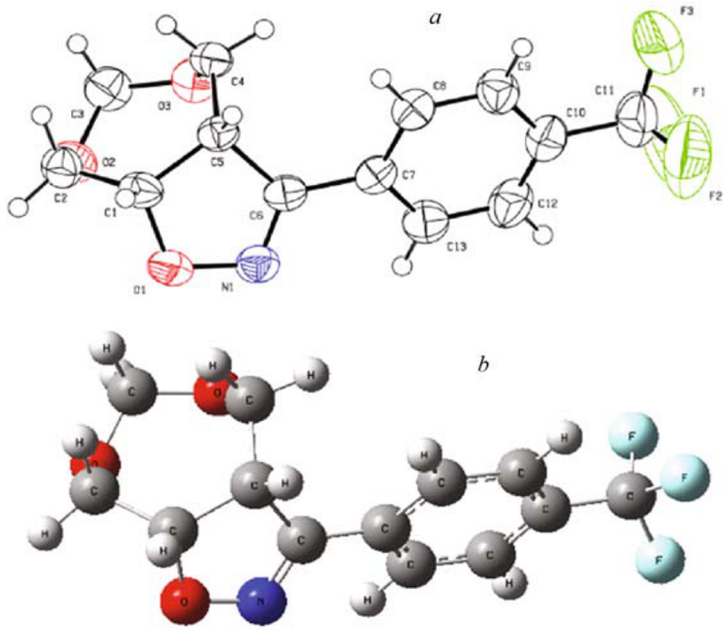

Fig. 1. (a) Experimental and (b) optimized structure with B3LYP/6-311++G(*d*,*p*) of OXE–OXA.

TABLE 1. Crystal Data, Collection, and Refinement Details

Empirical formula	$C_{13}H_{12}F_3NO_3$	Crystal size, mm	0.066 × 0.193 × 0.457
Formula weight	287.24	Crystal color	colorless block
Temperature, K	296(2)	θ range, deg	2.08–25.00
Wavelength, Å	0.71073	*h*, *k*, *l* range	$-12 \le h \le 11$
Crystal system	monoclinic		$-7 \le k \le 7$
Space group	*P*1 21/*n*1		$-22 \le l \le 23$
a, Å	10.314(2)	Reflection collected	7496
b, Å	6.2515(11)	Independent reflections	2231 [*R*(int) = 0.0613]
c, Å	19.962(4)	Data/restraints/parameters	2231/0/181
α, deg	90	Absorption correction	multi-scan
β, deg	100.761(16)	T_{max}/T_{min}	0.9910–0.9410
γ, deg	90	Refinement method	Full-matrix least-squares on F^2
Volume, Å^3	1264.5(4)	Final *R* indices [$I > 2\sigma(I)$]	$R_1 = 0.0707$, w$R_2 = 0.2019$
Z	4	*R* indices (all data)	$R_1 = 0.1044$, w$R_2 = 0.2335$
Density (calculated), g/cm^3	1.509	Goodness-of-fit on F^2	1.071
Absorption coefficient, mm^{-1}	0.136	Largest diff. peak and hole, e.Å^{-3}	0.555 and –0.424
F(000)	592	CCDC deposit number	2,100,835

TABLE 2. Experiment and Optimized Geometrical Parameters [bond lengths (Å), bond angles (deg), and dihedral angles (deg)] of OXE–OXA

Parameters	Exp.	Theoretical		Parameters	Exp.	Theoretical		Parameters	Exp.
Bond lengths	X-Ray	B3LYP	HSEh1PBE	Bond angles	X-Ray	B3LYP	HSEh1PBE	Dihedral angles	X-Ray
C_1–O_1	1.460(4)	1.458	1.447	C_{13}–C_7–C_6	120.6(3)	120.271	120.243	C_8–C_9–C_{10}–C_{11}	179.8(4)
C_1–C_5	1.536(5)	1.550	1.541	C_9–C_8–C_7	120.3(3)	120.848	120.768	C_9–C_{10}–C_{11}–F_1	–151.6(5)
C_2–O_2	1.417(4)	1.418	1.407	C_{12}–C_{10}–C_9	119.8(4)	119.976	120.121	C_9–C_{10}–C_{11}–F_3	–23.3(7)
C_3–O_3	1.403(5)	1.407	1.397	C_9–C_{10}–C_{11}	120.6(4)	120.215	120.239	C_9–C10–C_{11}–F_2	88.2(5)
C_4–C_5	1.512(5)	1.539	1.530	F_1–C_{11}–F_2	104.1(5)	107.160	107.309	C_1–C_{10}–C_{12}–C_{13}	–179.8(4)
C_6–C_7	1.471(5)	1.471	1.464	F_1–C_{11}–C_{10}	112.4(4)	112.354	112.242	C_8–C_7–C_{13}–C_{12}	–1.3(6)
C_7–C_8	1.393(5)	1.401	1.397	C_{12}–C_{13}–C_7	120.7(4)	120.624	120.514	C_7–C_6–N_1–O_1	–179.9(3)
C_{10}–C_{11}	1.471(6)	1.503	1.498	N_1–O_1–C_1	109.8(2)	110.474	110.601	C_6–N_1–O_1–C_1	–3.3(4)
C_{11}–F_3	1.324(6)	1.359	1.349	C_3–O_3–C_4	114.0(3)	115.171	114.800	C_5–C_1–O_1–N_1	6.1(3)
C_{12}–C_{13}	1.377(6)	1.386	1.383	O_1–C_1–C_5	105.0(3)	104.859	104.998	C_1–C_2–O_2–C_3	–81.1(4)
C_1–C_2	1.511(5)	1.527	1.519	C_6–C_5–C_1	100.3(3)	100.158	99.925	C_5–C_4–O_3–C_3	87.2(4)
C_3–O_2	1.394(4)	1.402	1.393	N_1–C_6–C_5	114.4(3)	113.561	113.397	C_5–C_1–C_2–O_2	61.3(4)
C_4–O_3	1.429(4)	1.418	1.407	C_{13}–C_7–C_8	118.9(4)	118.666	118.842	O_3–C_4–C_5–C_1	–58.7(4)
C_5–C_6	1.507(5)	1.521	1.511	C_8–C_7–C_6	120.6(3)	121.054	120.906	C_2–C_1–C_5–C_6	–125.4(3)
C_6–N_1	1.275(4)	1.281	1.278	C_8–C_9–C_{10}	120.1(4)	119.811	119.730	C_2–C_1–C_5–C_4	–2.7(5)
C_7–C_{13}	1.390(5)	1.404	1.400	C_{12}–C_{10}–C_{11}	119.6(4)	119.755	119.589	C_1–C_5–C_6–N_1	4.8(4)
C_8–C_9	1.380(5)	1.391	1.388	F_1–C_{11}–F_3	108.3(5)	106.492	106.663	C_1–C_5–C_6–C_7	–176.6(3)
C_9–C_{10}	1.388(5)	1.393	1.389	F_3–C_{11}–F_2	98.6(5)	106.413	106.549	C_5–C_6–C_7–C_{13}	–156.4(3)
C_{10}–C_{12}	1.380(6)	1.398	1.394	F_3–C_{11}–C_{10}	114.8(4)	111.833	111.712	C_5–C_6–C_7–C_8	23.2(5)
C_{11}–F_1	1.248(6)	1.352	1.343	C_{13}–C_{12}–C_{10}	120.1(4)	120.074	120.026	C_6–C_7–C_8–C_9	–178.3(3)
C_{11}–F_2	1.349(6)	1.352	1.343	C_6–N_1–O_1	110.1(3)	110.939	111.064	C_8–C_9–C_{10}–C_{12}	–0.2(6)
N_1–O_1	1.397(4)	1.381	1.363	C_3–O_2–C_2	114.9(3)	115.713	115.363	C_{12}–C_{10}–C_{11}–F_1	28.4(7)
Bond angles	X-Ray	B3LYP	HSEh1PBE	Dihedral angles	X-Ray	B3LYP	HSEh1PBE	C_{12}–C_{10}–C_{11}–F_3	156.7(5)
O_1–C_1–C_2	106.7(3)	108.267	108.189	O_1–C_1–C_2–O_2	–57.1(4)	–62.739	–61.530	C_{12}–C_{10}–C_{11}–F_2	–91.7(6)
C_2–C_1–C_5	118.9(3)	118.595	118.132	O_3–C_4–C_5–C_6	57.1(4)	54.009	52.775	C_9–C_{10}–C_{12}–C_{13}	0.2(6)
O_2–C_2–C_1	114.9(3)	114.585	114.364	O_1–C_1–C_5–C_6	–6.1(3)	0.877	1.005	C_8–C_9–C_{10}–C_{11}	179.8(4)
O_2–C_3–O_3	113.8(3)	114.396	114.505	O_1–C_1–C_5–C_4	116.5(3)	124.928	124.274	C_9–C_{10}–C_{11}–F_1	–151.6(5)
O_3–C_4–C_5	113.0(3)	113.945	113.769	C_4–C_5–C_6–N_1	–120.5(3)	–126.378	–125.790	C_9–C_{10}–C_{11}–F_3	–23.3(7)
C_6–C_5–C_4	113.1(3)	114.313	113.876	C_4–C_5–C_6–C_7	58.2(5)	54.199	54.532	C_9–C_{10}–C_{11}–F_2	88.2(5)
C_4–C_5–C_1	116.8(3)	116.901	116.777	N_1–C_6–C_7–C_{13}	22.2(5)	24.579	22.870	C_{11}–C_{10}–C_2–C_{13}	–179.8(4)
N_1–C_6–C_7	119.9(3)	120.199	120.389	N_1–C_6–C_7–C_8	–158.2(3)	–154.249	–155.994	C_8–C_7–C_{13}–C_{12}	–1.3(6)
C_7–C_6–C_5	125.7(3)	126.237	126.214	C_{13}–C_7–C_8–C_9	1.3(5)	–0.113	0.007	C_7–C_6–N_1–O_1	–179.9(3)

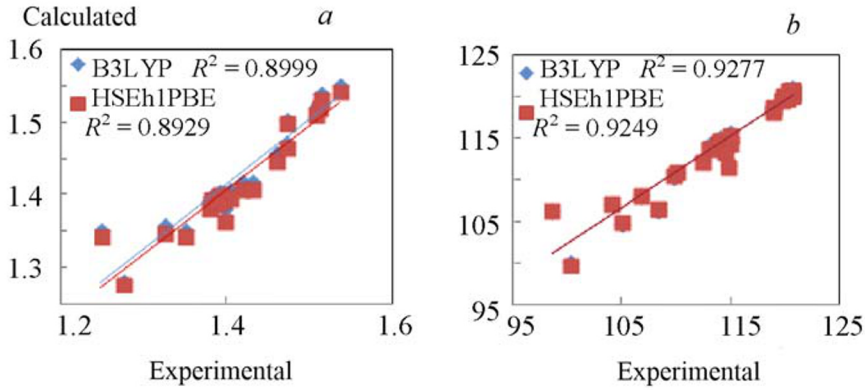

Fig. 2. Correlation graphics of experimental and calculated (with 6-311++G(*d*,*p*) level) molecular bond lengths (a) and molecular bond angles of OXE–OXA (b).

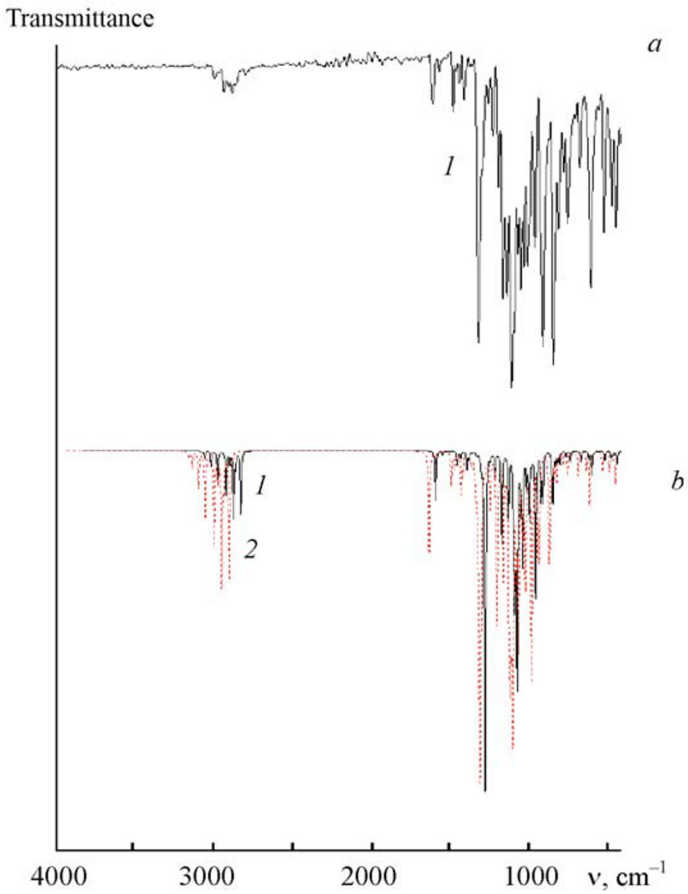

Fig. 3. (a) Experimental (FT-IR) and (b) calculated IR spectra of OXE–OXA, B3LYP/6-311+G(*d*,*p*) (1), HSEh1PBE/6-311+G(*d*,*p*) (2).

The theoretical and experimental vibrational frequencies and assignments of OXE–OXA compound are listed in Table 3. We made the vibrational band assignments using the GaussView molecular visualization program [25].

Optimized molecular geometric structural data were used to calculate the harmonic vibrational frequencies. The harmonic vibrational frequencies were scaled using scaling factors of 0.961 [32] for the B3LYP/6-311++G(*d*,*p*) method

TABLE 3. Experimental and Calculated Vibrational Frequencies and Assignments

Assignments	Experimental	B3LYP/6-311++G(*d*,*p*)		HSEh1PBE/6-311++G(*d*,*p*)	
		Unscaled freq.	Scaled freq.	Unscaled freq.	Scaled freq.
ν(C–H)	2999	3038	2920	3159	3026
ν_S(C–H_2)	2936	2989	2872	3062	2933
ν_S(C–H_2)	2883	2940	2826	3005	2879
ν(C=N), aromatic ν(C=C)	1605	1645	1581	1690	1619
aromatic ν(C=C)	1558	1603	1540	1678	1608
δ(C–H_2)	1479	1490	1432	1564	1499
ν(C–C_{F3})	1320	1326	1274	1398	1339
ν (C–C_{F3}), t(C–H_2), ρ(C–H)	1225	1251	1203	1289	1235
aromatic ρ(C–H)	1163	1206	1159	1255	1202
w(C–C_{F3})	1109	1121	1077	1189	1139
ν(N–O–C)	957	974	936	1002	960
ν(N–O), ρ(C–H_2)	908	933	896	974	933
aromatic w(C–H)	843	868	834	899	861
ρ(C–H_2), w(C–H)	604	607	584	647	620
ρ(C–H_2), w(C–H)	521	523	503	582	557
ρ(C–H_2)	440	444	426	473	454

Note. Vibrational modes: ν, stretching; a, asymmetric; s, symmetric; ρ, rocking; δ, scissoring; w, wagging; t, twisting; τ, torsion.

TABLE 4. Experimental and Calculated ^{13}C and ^{1}H Isotropic NMR Chemical Shifts (all values in ppm)

Atom	Experimental	B3LYP /6-311++G(*d*,*p*)	HSEh1PBE /6-311++G(*d*,*p*)
^{1}H			
H_{-C12}	7.805	8.391	8.658
H_{-C9}	7.787	7.822	8.036
H_{-C13}	7.709	7.764	7.975
H_{-C8}	7.609	7.198	7.437
H_{-C3}	4.983	5.035	5.101
H_{-C1}	4.957	4.706	4.830
H_{-C3}	4.639	4.512	4.687
H_{-C2}	4.424	4.499	4.617
H_{-C4}	4.178	4.188	4.205
H_{-C2}	4.053	3.707	3.804
H_{-C4}	4.042	3.510	3.606
H_{-C5}	3.944	3.500	3.592

TABLE 4. (Continued)

Atom	Experimental	B3LYP /6-311++G(*d*,*p*)	HSEh1PBE /6-311++G(*d*,*p*)
^{13}C			
C_6	156.349	160.173	153.223
C_7	132.361	140.112	133.795
C_{10}	131.955	137.305	131.218
C_{13}	131.629	134.224	128.466
C_{12}	127.432	133.848	126.516
C_{11}	127.232	131.743	124.956
C_9	126.132	129.914	124.716
C_8	125.889	128.782	123.512
C_3	98.573	103.357	96.448
C_1	84.037	89.761	82.190
C_2	69.128	74.723	68.044
C_4	66.386	71.025	64.308
C_5	51.774	55.967	48.104

and 0.958 [33, 34] for the HSEh1PBE/6-311++G(*d*,*p*) method. In the FT-IR spectrum (Fig. 3a), the C–H stretching band was observed at 2999 cm^{-1}. We calculated the theoretical C–H stretching band at 2920 cm^{-1} for B3LYP and 3026 cm^{-1} for HSEh1PBE. The experimental aromatic C=C stretching vibration peak was observed at 1558 cm^{-1}. We calculated this peak as 1540 cm^{-1} for B3LYP and 1608 cm^{-1} for HSEh1PBE. According to the results of the harmonic vibration calculation, we observed that the vibrational frequencies calculated using the HSEh1PBE method were closer to the experimental vibrational frequencies than those calculated using the B3LYP method.

^{1}H and ^{13}C nuclear magnetic resonance (NMR) spectra. Theoretical chemical shifts were calculated using two different DFT methods. The experimental and theoretical ^{1}H and ^{13}C chemical shifts of the OXE–OXA compound are listed Table 4 where these chemical shifts for ^{1}H and ^{13}C are reported and the atom statues are numbered according to Fig. 1a. We observed experimental ^{13}C chemical shift values in the range of ~156 to ~52 ppm as seen in Table 4. We calculated the theoretical ^{13}C chemical shift values for the OXE–OXA compound in the range of ~160 to ~56 ppm for B3LYP and ~153 to ~48 ppm for HSEh1PBE. The experimental ^{1}H chemical shift values were observed in the range of ~7.8 to ~3.9 ppm as seen in Table 4. We calculated the theoretical ^{1}H chemical shifts for OXE–OXA compound in the range of ~8.3 to ~3.5 ppm for B3LYP and ~8.7 to ~3.6 ppm for HSEh1PBE.

Conclusions. We experimentally and theoretically examined the molecular geometric parameters (bond lengths, bond angles and torsion angles) and spectroscopic (FT-IR and ^{1}H and ^{13}C NMR) analysis of the 3-[4-(trifluoromethyl) phenyl]-3a,4,8,8a-tetrahydro-6H-[1,3]dioxepino[5,6-d][1,2]oxazole (OXE–OXA) compound. We optimized our theoretical molecular modeling calculations for the OXE–OXA compound with two different DFT methods and the calculations demonstrated a strong correlation with our experimental results. The optimized geometric structure, the harmonic vibrational (FT-IR) frequencies and the results of ^{1}H and ^{13}C NMR chemical shifts seem to be in strong agreement with our experimental data.

REFERENCES

1. B. Prugoveki, M. Marinkovi, M. Vinkovi, and M. Dumi, *Croatica Chem. Acta C*, **79**, 219–226 (2006).
2. W. Gul, P. Carvalho, A. Galal, M. A. Averyb, and M. A. El Sohly, *Acta Cryst*., **65**, 358–359 (2009).
3. D. Palla, A. I. Antoniou, M. Baltas, C. Menendez, P. Grellier, E. Mouray, and C. M. Athanassopoulos, *Molecules*, **25**, Article ID 4858 (2020).

4. C. H. Lakshmi Praveena, V. Esther Rani, Y. N. Spoorthy, and L. K. Ravindranath, *J. Chem. Pharm. Res*., **5**, 280–292 (2013).
5. R. S. Pavelyev, R. M. Vafina, K. V. Balakin, O. I. Gnezdilov, A. B. Dobrynin, O. A. Lodochnikova, R. Z. Musin, G. A. Chmutova, S. A. Lisovskaya, and L. E. Nikitina, *Hindawi J. Chem*., **14**, Article ID 3589342 (2018).
6. E. Rani, M. Rani, and L. K. Ravindranath, *J. Med. Org. Chem*., **3**, 11–20 (2016).
7. S. Jana, S. Iram, J. Thomas, M. Q. Hayat, C. Pannecouque, and W. Dehaen, *Molecules*, **22**, 303 (2017).
8. H. Deng, X. Huang, C. Jin, C. M. Jin, and Z. S. Quan, *Bioorg. Chem*., **94**, Article ID 103467 (2020).
9. N. T. Giang, D. T. Tuyet Anh, H. T. Phuong, N. Thanh, and N. Tuyen, *Vietnam J. Chem*., **56**, 167–171 (2018).
10. K. V. Chikkula and S. Raja, *Int. J. Pharm. Pharm. Sci*., **9**, 13–24 (2017).
11. A. Shaik, R. R. Bhandare, K. Palleapati, S. Nissankararao, V. Kancharlapalli, and Shahanaaz Shaik, *Molecules*, **25**, 1047 (2020).
12. A. Banerjee, S. Bandyopadhyay, A. Gayen, T. Sengupta, A. Das, G. K. Chatterjee, and S. K. Chaudhuri, *Arzneimittel-forschung*, **44**, 863–866 (1994).
13. K. V. Chikkula and R. Sundararajan, *Med. Chem. Res*., **26**, 3026–3037 (2017).
14. R. Chaithra, S. Kumar, T. Pramila, and D. N. Vidya, *EJPMR*, **6**, 274–281 (2019).
15. Y. Kara and S. Yalduz, *J. Mol. Struct*., **1193**, 158–165 (2019).
16. APEX2, version 2014.11-0, Bruker (2014) Bruker AXS Inc., Madison
17. SAINT, version 8.34A, Bruker (2013) Bruker AXS Inc., Madison
18. SADABS, version 2014/5, Bruker (2014) Bruker AXS Inc., Madison
19. G. M. Sheldrick, *Acta Crystallogr. A*, **A71**, 3 (2015).
20. G. M. Sheldrick, *Acta Crystallogr. C*, **C71**, 3 (2015).
21. O. V. Dolomanov, L. Bourhis, R. J. Gildea, A. K. Howard, and H. Puschmann, *J. Appl. Crystallogr*., **42**, 339–341 (2009).
22. A. L. Spek, *J. Appl. Crystallogr.*, **36**, 7–11 (2003).
23. C. F. Macrae and I. Sovago, *J. Appl. Crystallogr*., **53**, 226 (2019).
24. M. J. Frisch, G. W. Trucks, H. B. Schlegel, et al., Fox, Gaussian 09, Revision A.1, Gaussian, Inc., Wallingford CT (2009).
25. GaussView, Version 5, Roy Dennington, Todd Keith, and John Millam, Semichem Inc., Shawnee Mission KS (2009).
26. A. D. Becke, *J. Chem. Phys*., **98**, Article ID 5648 (1993).
27. C. Lee, W. Yang, and R. G. Parr, *Phys. Rev. B*, **37**, 785 (1988).
28. J. Heyd and G. Scuseria, *J. Chem. Phys*., **121**, Article ID 1187 (2004).
29. J. Heyd and G. E. Scuseria, *J. Chem. Phys*., **120**, Article ID 7274 (2004).
30. J. Heyd, J. E. Peralta, G. E. Scuseria, and R. L. Martin, *J. Chem. Phys*., **123**, Article ID 174101 (2005).
31. J. Heyd, G. E. Scuseria, and M. Ernzerhof, *J. Chem. Phys*., **124**, Article ID 219906 (2006).
32. D. Avcı, S. Bahceli, O. Tamer, and Y. Atalay, *Can. J. Chem*., **93**, 1147 (2015).
33. H. Pir Gumus, O. Tamer, D. Avcı, and Y. Atalay, *J. Phys*., **90**, 1 (2015).
34. S. Sevvanthi, S. Muthu, S. Aayisha, P. Ramesh, and M. Raja, *Chem. Data Coll.*, **30**, Article ID 100574 (2020).